American Mineralogist, Volume 73, pages 1285–1291, 1988

Experimental evaluation of the $MnCO_3 + SiO_2 = MnSiO_3 + CO_2$ equilibrium at 1 kbar

JÜRGEN ABRECHT
Mineralogical Institute, University of Basel, Bernoullistrasse 30, CH-4056 Basel, Switzerland

ABSTRACT

The reaction $MnCO_3 + SiO_2 = MnSiO_3 + CO_2$ was investigated at 1-kbar pressure at temperatures between 390 and 485 °C by using hydrothermal techniques in a CO_2-H_2O mixture. Equilibrium conditions for the reaction, determined from reversed experiments, were used to derive an entropy 113 ± 6 J/(mol·K) and a Gibbs free energy of formation of −1237 ± 3 kJ/mol for the manganese silicate phase $MnSiO_3$ (pyroxenoid). Metastable pyroxmangite was obtained in the decarbonation reaction. Shape and surface textures of experimental products suggest a dissolution-(re)precipitation mechanism for the reaction. The obtained T-X_{CO_2} curve indicates nonideal-mixing behavior of the CO_2-H_2O fluid at the experimental P-T conditions.

INTRODUCTION

Rhodonite ($MnSiO_3$) and its polymorph pyroxmangite occur in both regional and contact-metamorphic rocks and also in metasomatites formed from carbonates subjected to either low-grade regional or very high-grade contact-metamorphic conditions. For the end-member $MnSiO_3$ composition, the pyroxmangite structure has been shown to be stable below approximately 400 °C, at pressures less than 2 kbar, whereas at higher temperatures, rhodonite is the stable phase (Maresch and Mottana, 1976). So far, no quantitative data are available on the commposition-stability relationships of rhodonite and pyroxmangite solid solutions. The most important cation exchanges in these solutions can be described by the $MnCa_{-1}$, $MnFe_{-1}$, and $MnMg_{-1}$ exchange operators. However, natural assemblages and experimental data (Abrecht and Peters, 1975) suggest that the rhodonite structure is stabilized with respect to that of pyroxmangite by Ca, whereas Fe and Mg increase the stability of pyroxmangite with respect to rhodonite. Whether rhodonite or pyroxmangite is the stable phase at a given P-T condition is primarily determined by the bulk composition of the rock.

Thermodynamic data derived from hydrothermal experiments on the equilibrium

$$\text{rhodochrosite} + \text{quartz} = \text{pyroxenoid} + CO_2 \quad (1)$$

were presented for pyroxmangite by Candia et al. (1975). They calculated a $\Delta G^0_{(1,298)} = -1238$ and -1243 kJ/mol from experiments carried out at 500 bars and 2000 bars, respectively (symbols are given in Table 1). They used an entropy $S^0 = 102.5$ J/(mol·K) taken from the rhodonite values tabulated by Robie and Waldbaum (1968). Winter et al. (1981) used the ΔG_f of Candia et al. (1975) in combination with thermochemical data tabulated by Robie et al. (1978) to calculate the univariant curve in T-X_{CO_2} space corresponding to the equilibrium of Reaction 1. Winter et al. (1981) observed a large discrepancy in the slope of this curve and the slope obtained by the experiments of Peters (1971). Since the tabulated thermochemical data are for rhodonite, these authors corrected for the entropy of pyroxmangite with the inversion data by Maresch and Mottana (1976), which yielded a $\Delta S_r = 1.2$ J/(mol·K). However, the experimental curve suggests a ΔS_r of about 330 J/(mol·K)! From the experiments by Maresch and Mottana (1976), the difference in the free energy of formation between the two phases is calculated to be only 430 J/mol. Because of these very small differences in the entropies and the Gibbs free energy, the T-X_{CO_2} curves for Reaction 1 differ by less than 3 °C for the two polymorphs. This means that within the expected experimental errors, the two curves cannot be distinguished, and, therefore, it is of no importance which $MnSiO_3$ pyroxenoid is used to determine thermochemical data such as entropy and Gibbs free energy.

EXPERIMENTAL PROCEDURES

The experiments were performed in Tuttle cold-seal bombs using sealed $Ag_{70}Pd_{30}$ capsules in all experiments. Some experiments were conducted under the oxygen-fugacity conditions of the graphite-methane buffer (G-CH_4 buffer), but others were buffered only by the pressure-vessel walls (~NNO buffer). For the graphite-methane buffer, the pressure medium was methane, and graphite was inserted into the pressure vessel as a filler rod (Huebner, 1971). The f_{O_2} of the G-CH_4 buffer at around 400 °C is about 2 log units lower than that of the NNO buffer. Despite possible equilibrium problems with the G-CH_4 buffer at low temperatures (Chou, 1987), the f_{O_2} buffer capacity was sufficient to prevent oxidation of the Mn inside the capsule. No differences were detected in experimental products as a result of the use of different buffers. CO_2-H_2O mixtures in the experiments were generated by adding weighed amount of $Ag_2C_2O_4$ and H_2O to the capsules or, for mixtures in which $X_{CO_2} = 0.5$, directly by the decomposition of oxalic acid dihydrate. After completion of the experiment, CO_2 weight was determined as the weight difference before and immediately after puncturing of a capsule. H_2O weight was then determined as the weight difference of the capsule immediately after puncturing and after subsequent drying at 110 °C. To minimize the escape of H_2O with the CO_2 gas (Kerrick,

0003–004X/88/1112–1285$02.00

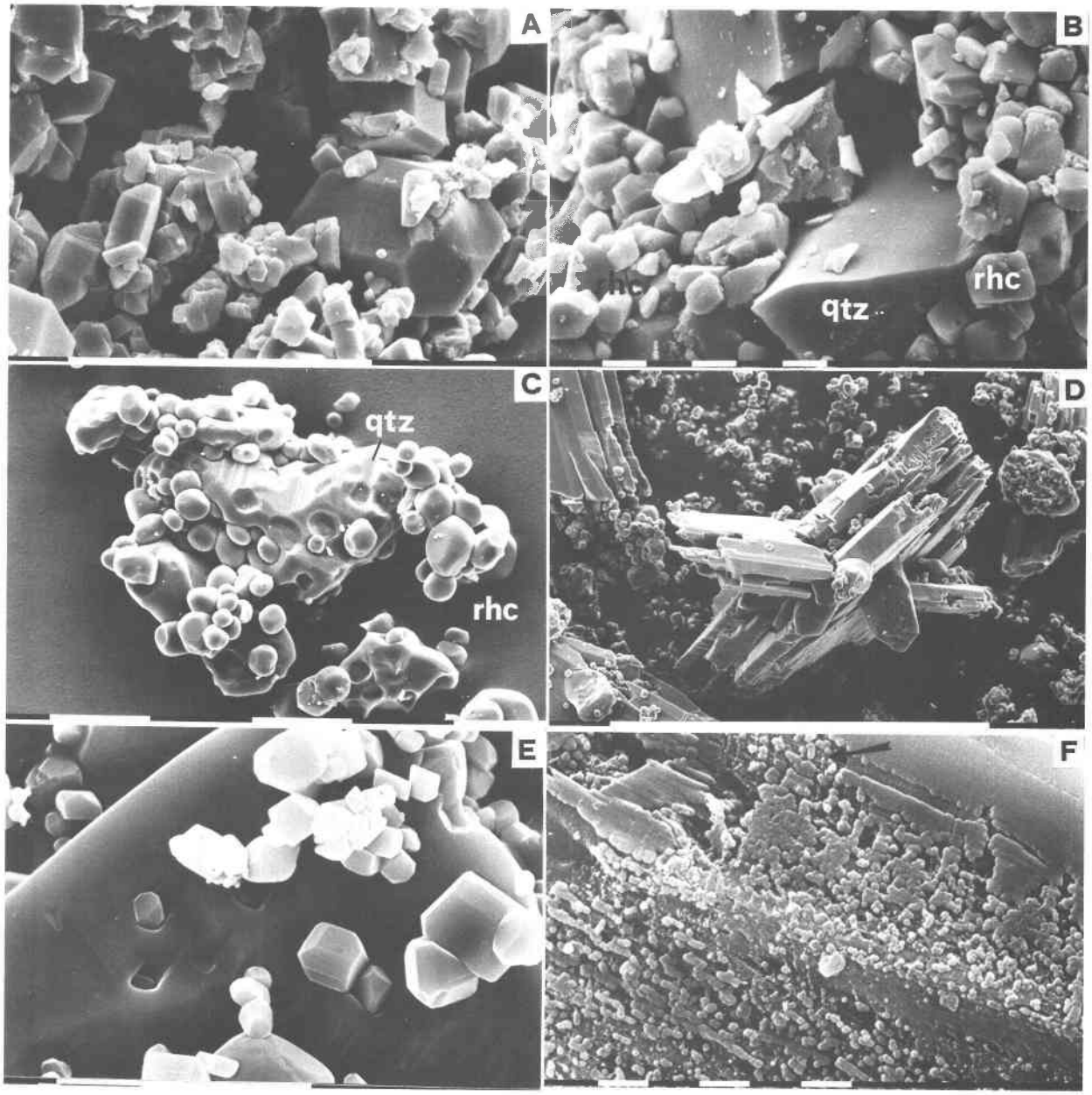

Fig. 1. SEM backscattered electron images of educts and products of hydrothermal experiments. (**A**) Starting mix B: Rhodonite, hydrothermally synthesized at 800 °C (scale bar = 10 μm). (**B**) Starting mix A: Rhodochrosite crystals (rhc) and xenomorphic quartz grains (qtz) (scale bar = 1 μm). (**C**) Quartz with stepwise growth features and impressions of round carbonate crystals. Run R26: $T = 450$ °C, $X_{CO_2} = 0.48$, no silicate formed (scale bar = 10 μm). (**D**) Pyroxmangite grown at $T = 441$ °C and $X_{CO_2} = 0.26$. Larger roundish grains are quartz with small carbonate crystals (scale bar = 0.1 mm). (**E**) Recrystallized rhodochrosite (partly overgrown) on top of quartz with striated faces. Run R101: $T = 391$ °C, $X_{CO_2} = 0.025$ (scale bar = 10 μm). (**F**) Pyroxmangite with formation of small spheres on surface growing into strings and eventually into new layers. Note the bimodal size distribution of the spheres (black arrow at top). Run R101: $T = 391$ °C, $X_{CO_2} = 0.025$ (scale bar = 1 μm).

1974), a thin paper tissue, slightly larger than the capsule, was wrapped around the capsule before puncturing, thereby soaking up any escaping H_2O. An accuracy of +2 mol% CO_2 is assumed on the basis of two experiments with only the oxalic acid. The gas in the capsule in all experiments was assumed to be essentially a binary H_2O-CO_2 mixture possibly with very low amounts of CO and CH_4 (Greenwood, 1967a; Kerrick, 1974). Capsules showing weight loss or gain during an experiment were discarded. Products were examined by using X-ray diffraction, optical methods including phase-contrast microscopy, and the scanning electron microscopy (SEM).

Rhodonite was synthesized either from oxide mixes (MnO_2 or

MnO and SiO_2 glass) or from stoichiometric $MnCO_3 + SiO_2$ mixtures. The synthesis conditions were 750 to 800 °C and a pressure of 1 kbar. Cell parameters for the synthetic rhodonite are (in Å) $a = 7.624(2)$, $b = 11.852(4)$, $c = 6.710(1)$, and $\alpha = 92.32$, $\beta = 94.47$, $\gamma = 105.68$, $V = 580.8(3)$ Å^3 for space group $P\bar{1}$. For product pyroxmangite (sample no. RR89), the following cell parameters were measured (for space group P_1): $a = 6.707(3)$, $b = 7.594(2)$, $c = 17.405(11)$, and $\alpha = 113.68$, $\beta = 82.43$, $\gamma = 94.65$, $V = 804.4(6)$ Å^3. The grains were well crystallized (Fig. 1a), and no impurities were detected. The size range of the synthetic pyroxmangite grains was 5–10 μm. The rhodochrosite was obtained by treating freshly precipitated (with K_2CO_3) $MnCO_3$ at 300 °C at $P_{CO_2} = 800$ bars. The resulting rhodochrosite showed distinct and sharp X-ray diffraction peaks. The grain size of the carbonate was around 1–2 μm. A natural optical-grade quartz from Brazil, having an average grain size of about 10 μm, was used. The stoichiometric starting mix was ground by hand under acetone in an agate mortar for about ½ h.

Results

The critical experimental data for the reaction $MnCO_3 + SiO_2 = MnSiO_3 + CO_2$ are given in Table 2. The amounts of experimental products (i.e., newly formed phases) were estimated optically and varied greatly between ≤1% and >75%. This variation is probably due to the relatively short durations of the experiments and to kinetic barriers for experiments close to equilibrium conditions. Experiments not showing any reaction products are not listed and were not used for calculations.

Figure 2 shows the equilibrium curve consistent with the reversal brackets at 1 kbar given in Table 2. The reaction product obtained from rhc + qtz was always pyroxmangite, which according to Maresch and Mottana (1976) is only stable below 400 °C. The formation of metastable pyroxmangite within the rhodonite stability field has been observed in other experimental studies (Peters, 1971; Abrecht and Peters, 1975; Momoi, 1974). This metastable formation also holds for Ca-bearing compositions (Abrecht, 1984). The problem may be avoided by using seeded starting mixtures (Maresch and Mottana, 1976).

Reaction textures from SEM

The SEM pictures were not only useful in detecting newly grown phases, but they also enabled determination of reaction direction from surface textures and crystal shapes (Figs. 1A–1F).

Table 1. Symbols and abbreviations used

ΔG^0, ΔH^0	Standard Gibbs free energy of formation, standard enthalpy of formation
S^0	third-law entropy
ΔH_r, ΔS_r, ΔV_r	enthalpy of reaction, entropy of reaction, volume change of a reaction
ΔC_p	heat capacity
f	fugacity
K	equilibrium constant
rhc	rhodochrosite
qtz	quartz
rdn	rhodonite
pym	pyroxmangite

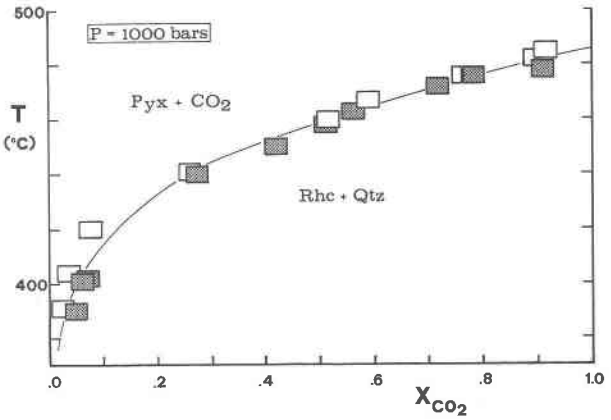

Fig. 2. T vs. X_{CO_2} diagram of experimental data. Empty symbols represent the reaction rhc + qtz → pyroxenoid + CO_2; shaded symbols represent the decarbonation reaction rdn + CO_2 → rhc + qtz. Size of the symbols approximately represents errors in X_{CO_2} and temperature.

The rhc + qtz starting mixture (mix A, Fig. 1B) consisted of xenomorphic quartz grains with sharp edges and conchoidal cleavage planes (1–15 μm in diameter). No crystal faces were observed in the starting materials. Carbonate grains were more uniform in size and usually occurred as fairly well crystallized simple rhombohedra (1–2 μm) with rounded edges (Fig. 1B). The rhodonite for the high-T starting material (mix B) was always well crystallized with grain sizes ranging from 1 to 10 μm (Fig. 1A). Grains were usually tabular to prismatic with well-developed crystal faces. Smaller grains were often overgrown by larger ones; no striated faces were observed.

Reactions with qtz + rhc starting mix (A). Hydrothermal treatment of mix A within the rhodochrosite-quartz

Table 2. Critical experimental data

Run	T (°C)	X_{CO_2}	Starting material	New formed product*	% Reaction**	Run time (d)
76	390	0.048	rdn	rhc + qtz	5	10
101	391	0.025	rhc + qtz	pym	<1	24
35	401	0.063	rdn	rhc + qtz	75	14
36	402	0.073	rdn	rhc + qtz	30	19
92	404	0.037	rhc + qtz	pym	<1	15
93	420	0.079	rhc + qtz	pym	2	13
84	440	0.274	rdn	rhc	2	13
67	441	0.258	rhc + qtz	pym	45	10
29	450	0.421	rdn	rhc + qtz	30	17
60	458	0.514	rhc + qtz	pym	50	15
88	460	0.516	rdn	rhc + qtz	5	24
27	463	0.561	rhc + qtz	pym	50	15
82	467	0.589	rdn	rhc + qtz	2	25
90	467	0.590	rhc + qtz	pym	80	25
58	473	0.719	rhc + qtz	pym	25	22
89	476	0.764	rhc + qtz	pym	80	31
86	476	0.794	rdn	rhc + qtz	5	31
40	482	0.894	rhc + qtz	pym	<1	23
54	478	0.909	rdn	rhc	<1	23
42	485	0.914	rhc + qtz	pym	<1	14

* Observed under optical microscope or SEM.
** Estimated under optical microscope.

stability field resulted in solution and reprecipitation of quartz, as indicated by the development of stepwise or striated faces (Fig. 1C) and, possibly, by quartz overgrowths on carbonate grains (Fig. 1E). The abundant roundish hollows on the quartz surface (Fig. 1C) are most likely dissolution phenomena. Very often they are occupied by carbonate grains that apparently induced higher quartz solubility along the quartz-carbonate grain contacts. This peculiar phenomenon was observed for all experiments and was especially obvious in experiments carried out at $X_{CO_2} > 0.5$. For textures formed within the pyroxenoid stability field, a striking feature is the shape of the carbonate grains as a function of the fluid composition. The development of rhodochrosite crystal faces is only observed in H_2O-rich fluids, where rhodochrosite grains show well-shaped combinations of rhombohedra and prisms with sharp edges (Fig. 1E). At $X_{CO_2} \geq 0.25$, grain edges are more rounded, but crystal faces are still visible, whereas at $X_{CO_2} > 0.50$, the grains are round, and crystal faces occur only rarely (Fig. 1C).

Newly formed pyroxmangite occurred as skeletal crystals with striated faces up to 0.1 mm long (Fig. 1D). Of special interest is the growth behavior of pyroxmangite in experiment R101, conducted at $X_{CO_2} = 0.03$. In this experiment, growth began with faceless (as far as observable) half spheres that first agglomerated into single ribbons and eventually formed continuous planes (Fig. 1F). The spheres show a bimodal size distribution; very small grains about 0.02 μm and larger ones about 0.1–0.2 μm, the size of which is interpreted as the upper size limit before agglomeration begins.

Reactions with rhodonite starting mix (B). The decomposition of rhodonite is indicated by the corrosion of prism end faces that produced teethlike forms. However, coexisting rhodonite crystals may still occur without any indication of dissolution. New carbonate grains preferentially formed on the surface of rhodonite and exhibit simple rhombohedral shapes comparable to those in the starting material mix A. The new quartz grains display the hexagonal-bipyramidal habit. These features strongly indicate a dissolution-(re)precipitation mechanism with a recrystallization of quartz and carbonate already at low temperatures and an increased solubility of rhodochrosite in the very H_2O-rich fluids. Unlike other comparable studies of reaction textures (e.g., Heinrich et al., 1986), no growth of the silicate phase on quartz or carbonate surfaces at high X_{CO_2} was observed. However, frequent quartz or carbonate grains partly included in pyroxmangite may have served as sites favorable to nucleation. The well-developed reactant rhodochrosite rhombohedra at $X_{CO_2} < 0.05$ indicate carbonate recrystallization and suggest increased solubility of this phase at these very H_2O-rich conditions. This agrees well with the results of Fein and Walther's (1986) experimental investigation of calcite solubility at $X_{CO_2} < 0.15$. Fein and Walther found increasing solubility of carbonate up to X_{CO_2} values between 0.01 and 0.07 and decreasing solubilities for more CO_2-rich compositions.

Calculation of S^0 and $\Delta G^0_{f(1,298)}$ of $MnSiO_3$ phase

As has been emphasized by several authors (e.g., Gordon and Greenwood, 1970; Kerrick and Slaughter, 1976), the change of entropy and enthalpy of a decarbonation reaction can be calculated from equations for ln K vs. $1/T$ curves using experimental data. Assuming that V_r, S_r, and H_r are constant, the equilibrium expression can be given as

$$\ln K = -\Delta H_r/RT + \Delta S_r/R - \Delta V_{sol}(P - 1)/RT. \quad (2)$$

If the standard state for the fluid is the pure nonideal gas at 1 bar and the temperature of interest, then

$$\ln K = \ln f_{CO_2}. \quad (3)$$

The standard state for the solid phase is 1 bar and T. However, if heat-capacity functions are available for all phases, the temperature dependence of the entropy and enthalpy of reaction can be evaluated and the ΔS^0_{298} *and* ΔH^0_{298} can be calculated by

$$\Delta G_{r(P,T)} = \Delta H^0_{298} - T\Delta S^0_{298} + \int_{298}^{T} \Delta C^0_P \, dT - T\int_{298}^{T} (\Delta C^0_P/T)\, dT + \int_1^P \Delta V^0 \, dP, \quad (3)$$

where

$$\int_{298}^{T} \Delta C^0_P \, dT = \Delta(H_T - H_{298}) \quad (3a)$$

$$\int_{298}^{T} (\Delta C^0_P/T)\, dT = \Delta(S_T - S_{298}) \quad (3b)$$

$$\int_1^P \Delta V^0 \, dP = \Delta V^0_{sol}(P - 1) + RT \ln f_{CO_2}. \quad (3c)$$

We can rearrange Equation 3 for equilibrium conditions and formulate it for $\log f$:

$$\log f_{CO_2} + \frac{\Delta V_{sol}(P - 1)}{2.303RT} + \frac{1}{2.303RT}\int_{298}^{T} \Delta C^0_P \, dT - \frac{1}{2.303R}\int_{298}^{T} (\Delta C^0_P/T)\, dT = \frac{\Delta H^0_{298}}{2.303RT} - \frac{\Delta S^0_{298}}{2.303R}. \quad (4)$$

The left-side terms of Equation 4 are combined as $\log f_{CO_2} + C$ and plotted versus the right-side terms and fitted to a straight line with $\Delta H^0_{298}/2.303R$ and $\Delta S^0_{298}/2.303R$ as constants (Fig. 3). By applying a Marquardt least-squares fit (Bevington, 1969) to the 1-kbar data, we can determine the error involved in our approach to measuring X_{CO_2}. An absolute error of ± 2 mol% CO_2 affects the log K to a higher degree at low X_{CO_2}, which explains the wide error bars given in Figure 3 for the low-temperature experiments. This fit yields an entropy of reaction at $T = 298.15$ °C of 185.3 ± 1.2 J/(mol·K). Using published entropy

data for quartz, rhodochrosite, and CO_2 (Robie et al., 1978; see Table 3), the S^0_{298} of the $MnSiO_3$ phase is calculated to be 113 ± 6 J/(mol·K), which is slightly higher than the number reported by Robie et al. (1978) [102.5 ± 2.1 J/(mol·K)]. In the new value, uncertainties in the tabulated thermochemical data are not taken into account.

The slope of the curve is very much determined by the points for $T \geq 440$ °C (Fig. 3). This is also indicated by Figure 2, which shows that the curve is well constrained at $X_{CO_2} > 0.2$ but somewhat less well constrained in the very H_2O-rich portion of the diagram.

Chatterjee (1977) and Kerrick and Slaughter (1976) have demonstrated that over a limited range of temperatures it is safe to assume that ΔS_r is constant. Indeed, a calculation of Reaction 1 by Equation 3 shows that the entropy of reaction decreases by only 2.7 J/(mol·K) between 380 and 480 °C. With the available data, we may use the following equation for the calculation of the standard Gibbs free energy of formation of $MnSiO_3$:

$$\Delta G_{(P,T)} = \Delta G^0_{(1,298)} - \int_{298}^{T} \left(\Delta S^0_{298} + \int_{298}^{T} (\Delta C^0_P/T)\, dT \right) dT + \int_1^P \Delta V^0\, dP. \quad (5)$$

The pressure term can be split as shown in Equation 3c. Setting Equation 5 equal zero, we may solve for $\Delta G^0_{f(1,298)}$ of $MnSiO_3$ for all the experimental points given in Table 2. The average of the values obtained is the preferred $\Delta G^0_{f(1298)}$of the pyroxenoid phase.

Using fugacity coefficients calculated with a modified Redlich-Kwong equation (Jacobs and Kerrick, 1981), a $\Delta G^0_{f(1,298)} = -1236.9 \pm 3$ kJ/mol is obtained from Equation 5, which is in good agreement with the tabulated value of 1243.1 ± 0.4 kJ/mol (Robie et al., 1978). The error of 3 kJ/mol for the new number is only due to the error involved in the S^0 of the pyroxenoid. By using the fugacity coefficient for CO_2 gas tabulated by Shmulovich and Shmonov (1975), the Gibbs free energy of formation obtained for the $MnSiO_3$ phase changes by less than 400 J/mol. For the other phases, the data given in Table 3 were used. For the reasons given before, one cannot tell

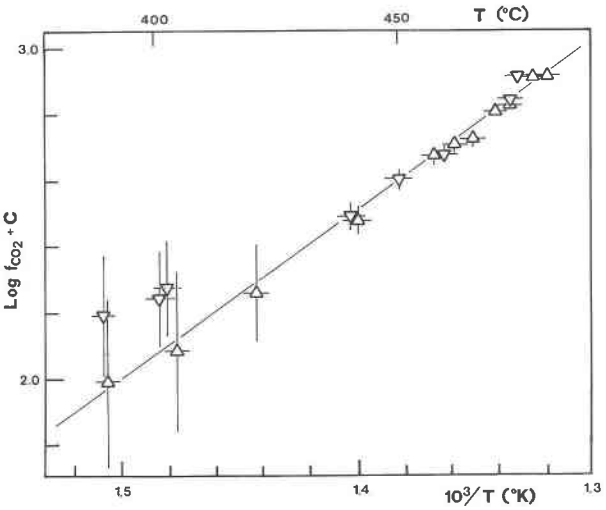

Fig. 3. Log f + C vs. $1/T$ diagram of 1-kbar experimental data with error bars. C comprises the terms on the left side of Equation 4 (see text). The curve has been fitted to the points by a least-square fitting method. Triangles represent the reaction rhc + qtz → pym + CO_2; upturned triangles, the reversed reaction.

for which $MnSiO_3$ polymorph the derived data are valid. But, by arbitrarily assuming that these data are valid for rhodonite, the corresponding data for the pyroxmangite phase can be calculated by using the inversion data of Maresch and Mottana (1976). The results are given in Table 3.

Calculation of T vs. X_{CO_2} curves

With the available data one can calculate T vs. X_{CO_2} curves at any pressure. The calculated curve for 1-kbar pressure, assuming ideal mixing, is shown together with the experimental curve in Figure 4.

The data presented in this paper require nonideal mixing behavior of the CO_2-H_2O fluid at the given P-T conditions. From experiments on the calcite-quartz-wollastonite-CO_2 equilibrium at 1 kbar, Greenwood (1967b) has concluded that nonideality is negligible. However, the calcite-quartz-wollastonite reaction takes place at distinctly higher temperatures, and the increase in nonideality with decreasing temperature is to be expected.

Table 3. Thermodynamic data used in this study

Phase	Reference*	V (J/bar)	S^0 (J/mol)	ΔG^0_f [kJ/(mol·K)]	Heat-capacity constants			
					a	$b \times 10^3$	$c \times 10^{-3}$	$d \times 10^{-5}$
Quartz	1	2.269	41.34	−856.2	46.94	34.31	−11.30	0.00
H_2O	1		188.72	−228.6	30.54	10.29	0.00	0.00
CO_2	1		213.69	−394.4	44.22	8.79	−8.62	0.00
$MnCO_3$	1	3.108	100.00	−816.1	92.01	38.911	−19.6230	1.4171
Rhodonite	2	3.498	102.51	−1243.1	99.04	19.145	−3.0407	2.7447
	3		113.0	−1236.9				
Pyroxmangite	4	3.461	111.8	−1237.3	99.04	19.145	−3.0407	2.7447

* References are as follows: (1) Helgeson et al. (1978). (2) Robie et al. (1978); molar volume from this study. (3) This study. (4) This study; C_P function from rhodonite. Calculated from experimental data of Maresch and Mottana (1976). See text.

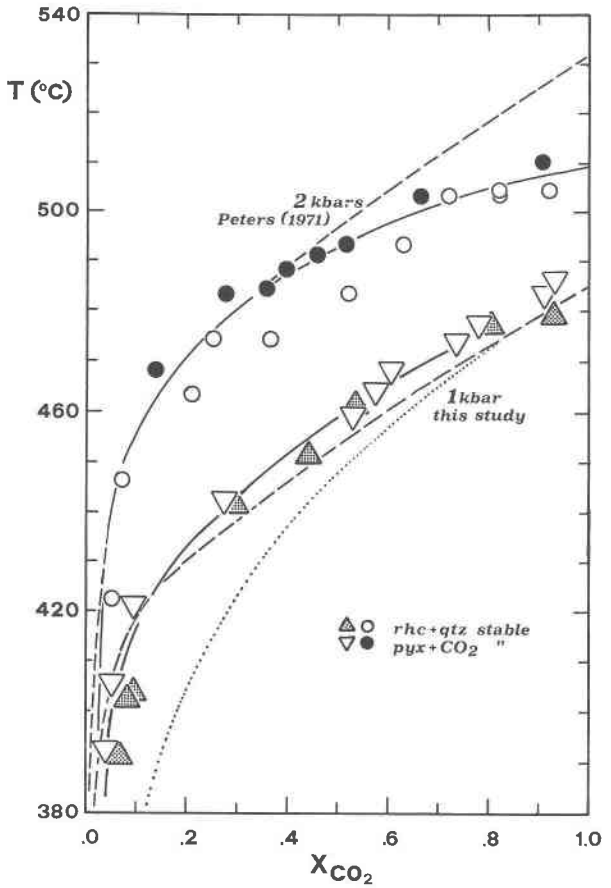

Fig. 4. Calculated and experimental T vs. X_{CO_2} curves at 1 kbar (this study) and 2 kbar (Peters, 1971). The dashed calculated curves are for nonideal fluid mixing (fugacity coefficients from MRK by Jacobs and Kerrick, 1981). The dotted curve is for ideal mixing at 1 kbar.

Previous experimental studies

The calculated equilibrium temperatures for Reaction 1 based upon the 1-kbar experiments differ from the experimental data of Peters (1971; 2 kbar) and Candia et al. (1975; 0.5 kbar). According to the new data, the 2-kbar equilibrium temperature in pure CO_2 is at about 530 °C, about 20 °C higher than that determined by Peters. At 0.5 kbar, our calculated temperature is lower by about 30 °C than that of Candia et al. (1975). Figure 4 shows that the calculated curve at 2-kbar pressure using Jacobs and Kerrick's MRK (1981) agrees very well with the experimental curve of Peters at $X_{CO_2} < 0.5$. At higher values of X_{CO_2}, the curve of Peters has a considerably flatter slope than the calculated equivalent (see Winter et al., 1981). This may explain the anomalous entropy datum obtained from his experiments (Table 3). At 500 bars, the agreement of the calculated curve with experimental data of Candia et al. (1975) is poor. However, the calculated curve shows a conspicuous minimum that most likely is due to problems with the calculated CO_2 fugacity coefficients. So far no explanation can be offered for the differing experimental results of Peters (1971) and Candia et al. (1975). The flat slope of the curve of Peters at high X_{CO_2} could possibly be explained by an additional fluid component positively correlated to the amount of CO_2 that caused erroneously high X_{CO_2}.

Acknowledgments

The experiments for this study have been performed at the Virginia Polytechnic Institute and State University, Blacksburg, Virginia, which also provided financial support. The study greatly benefited from critical reviews by S. R. Bohlen, E. J. Essene, H. J. Greenwood, M. Frey, D. A. Hewitt, T. Peters, T. Thoenen, and J. Connolly. W. Stern kindly provided X-ray data of the pyroxmangite. I am also very grateful for the help by the staff of the Labor für Rasterelektronenmikroskopie of the University of Basel.

References cited

Abrecht, J. (1984) Dehydration reactions of inesite, $Ca_2Mn_7Si_{10}O_{28}(OH)_2 \cdot 5H_2O$. Neues Jahrbuch für Mineralogie Monatshefte, 70–82.

Abrecht, J., and Peters, T. (1975) Hydrothermal synthesis of pyroxenoids in the system $MnSiO_3$-$CaSiO_3$ at $P_f = 2$ kb. Contributions to Mineralogy and Petrology, 50, 241–246.

Bevington, P.R. (1969) Data reduction and error analysis for the physical sciences. McGraw-Hill, New York.

Candia, M.A.F., Peters, T., and Valarelli, J.V. (1975) The experimental investigation of the reactions $MnCO_3 + SiO_2 = MnSiO_3 + CO_2$ and $MnSiO_3 + MnCO_3 = Mn_2SiO_4 + CO_2$ in CO_2/H_2O gas mixtures at a total pressure of 500 bars. Contributions to Mineralogy and Petrology, 52, 261–266.

Chatterjee, N.D. (1977) Thermodynamics of dehydration equilibria. In D.G. Fraser, Ed., Thermodynamics in geology, p. 137–160. Reidel, Boston.

Chou, I-M. (1987) Calibration of the graphite-methane buffer using the f_{H_2} sensors at 2-kbar pressure. American Mineralogist, 72, 76–81.

Fein, J.B., and Walther, J.V. (1986) The solubility of calcite in supercritical CO_2-H_2O fluids (abs.). EOS, 67, 388.

Gordon, T.M., and Greenwood, H.J. (1970) The reaction: dolomite + quartz + water = talc + calcite + carbon dioxide. American Journal of Science, 268, 225–242.

Greenwood, H.J. (1967a) Mineral equilibria in the system MgO-SiO_2-H_2O-CO_2. In P.H. Abelson, Ed., Researches in geochemistry, vol. 2, p. 542–567. Wiley, New York.

——— (1967b) Wollastonite: Stability in H_2O-CO_2 mixtures and occurrence in a contact-metamorphic aureole near Salmo, British Columbia, Canada. American Mineralogist, 52, 1669–1680.

Heinrich, W., Metz, P., and Bayh, W. (1986) Experimental investigation of the mechanism of the reaction: 1 tremolite + 11 dolomite = 8 forsterite + 13 calcite + 9 CO_2 + 1 H_2O. A SEM study. Contributions to Mineralogy and Petrology, 93, 215–221.

Helgeson, H.C., Delany, J.M., Nesbitt, H.W., and Bird, D.K. (1978) Summary and critique of the thermodynamic properties of rock-forming minerals. American Journal of Science, 278A, 1–229.

Huebner, J.S. (1971) Buffering techniques for hydrostatic systems at elevated pressures. In G.C. Ulmer, Ed., Research techniques for high pressure and temperature, p. 123–177. Springer, New York.

Jacobs, G.K., and Kerrick, D.M. (1981) APL and FORTRAN programs for a new equation of state for H_2O, CO_2, and their mixtures at supercritical conditions. Computers and Geosciences, 7, 131–143.

Kerrick, D.M. (1974) Review of metamorphic mixed-volatile (H_2O-CO_2) equilibria. American Mineralogist, 59, 729–762.

Kerrick, D.M., and Slaughter, J. (1976) Comparison of methods for calculating and extrapolating equilibria in P-T-$X(CO_2)$ space. American Journal of Science, 276, 883–916.

Maresch, W.V., and Mottana, A. (1976) The pyroxmangite-rhodonite transformation for the $MnSiO_3$ composition. Contributions to Mineralogy and Petrology, 55, 69–79.

Momoi, H. (1974) Hydrothermal crystallization of $MnSiO_3$ polymorphs. Mineralogical Journal, 7, 359–373.

Peters, T. (1971) Pyroxmangite: Stability in H_2O-CO_2 mixtures at a total pressure of 2000 bars. Contributions to Mineralogy and Petrology, 32, 267–273.

Robie, R.A., and Waldbaum, D.R. (1968) Thermodynamic properties of minerals and related substances at 298.15°K (25°C) and one atmosphere (1.013 bars) pressure and at higher temperature. U.S. Geological Survey Bulletin 1259.

Robie, R.A., Hemingway, B.S., and Fisher, J.R. (1978) Thermodynamic properties of minerals and related substances at 298.15 K and 1 bar (10^5 pascals) pressure and at higher temperatures. U.S. Geological Survey Bulletin 1452.

Shmulovich, K. I., and Shmonov, V.M. (1975) Fugacity coefficients for CO_2 from 1.032 to 10000 bar and 450–1300°K. Geochemistry International, 12, 202–206.

Winter, G.A., Essene, E.J., and Peacor, D.R. (1981) Carbonates and pyroxenoids from the manganese deposit near Bald Knob, North Carolina. American Mineralogist, 66, 278–289.

Manuscript received March 22, 1988
Manuscript accepted July 1, 1988